EXTRACTION OF THERMAL PERFORMANCE VALUES FROM SAMPLES IN THE LUNAR DUST ADHESION BELL JAR[*]

James R. Gaier and John Siamidis
NASA Glenn Research Center, Cleveland, OH 44135

Elizabeth M.G. Larkin
Case Western Reserve University, Cleveland, OH 44106

ABSTRACT

A simulation chamber has been developed to test the performance of thermal control surfaces under dusty lunar conditions. The lunar dust adhesion bell jar (LDAB) is a diffusion pumped vacuum chamber (10^{-8} Torr) built to test material samples less than about 7 cm in diameter. The LDAB has the following lunar dust simulant processing capabilities: heating and cooling while stirring in order to degas and remove adsorbed water; RF air-plasma for activating the dust and for organic contaminant removal; RF H/He-plasma to simulate solar wind; dust sieving system for controlling particle sizes; and a controlled means of introducing the activated dust to the samples under study. The LDAB is also fitted with an *in situ* Xe arc lamp solar simulator, and a cold box that can reach 30 K. Samples of thermal control surfaces (2.5 cm diameter) are introduced into the chamber for calorimetric evaluation using thermocouple instrumentation. The object of this paper is to present a thermal model of the samples under test conditions and to outline the procedure to extract the absorptance, emittance, and thermal efficiency from the pristine and sub-monolayer dust covered samples.

INTRODUCTION

On January 14, 2004, President George W. Bush outlined the Vision for Space Exploration which, among other goals, called for a "human return to the Moon by the year 2020" (ref. 1). The Vision for Space Exploration has since been formalized by Congressional legislation as the revised US Space Policy. This was fleshed out in more detail in the Exploration Systems Architecture Study (ref. 2), which calls for the first lunar landing to be in the year 2018. This is an ambitious schedule given that none of the launch or space vehicles called for by the study presently exist and there are budgetary constraints under which the program must be carried out. If the program is to be successful, it must build on the lessons learned during the first human lunar missions, those of the Apollo program.

One of the lessons learned during the Apollo program was that dust on the lunar surface posed a surprisingly broad array of difficulties (ref. 3). There were problems to varying degrees with vision obscuration, equipment clogging, dust coating and abrading, radiator performance degradation, seals failing, and dust inhalation. Apollo 17 astronaut Harrison Schmitt remarked at a lunar simulation workshop in 2005 that, "Dust is the number one environmental problem on the Moon" (ref. 4). These effects were a major concern even though the Apollo landers were on the lunar surface for no more than about three days. The early phases of the Exploration program envision missions of seven to fourteen days, with the eventual establishment of a permanent lunar base. Clearly the next human lunar surface missions must be better equipped to deal with dust.

A specific task has been set up under the Exploration program to develop technologies to mitigate the effects of lunar dust on surface missions. An important aspect of this technology development will be to test possible dust mitigation solutions in a simulated lunar environment on Earth. One of the lessons of Apollo is that these must be high fidelity tests. Dust mitigation technologies that were tested in simulation for Apollo did not always work on the Moon. For example, it was thought that using a nylon brush would be an effective way to remove lunar dust from the lunar roving vehicle (LRV) radiator surfaces (ref. 5). However, under lunar conditions the brush did not remove the very fine particles, and as a result the thermal performance of the radiator surfaces was degraded significantly in spite of brushing (refs. 6, 7, and 8).

Three strategies can be employed to mitigate the effects of dust on surface system components. First, components can be designed so that they can better tolerate the effects of dust. An example might be a space suit fabric that has better resistance to abrasion by lunar dust. Second, components can be designed such that less dust attaches to them. For example, a space suit fabric can have a smooth outer layer so that dust cannot so easily work its way between the fibers, so there is less dust on the fabric to abrade it. Third, techniques can be developed to clean dust from surfaces. Perhaps an air shower can be built into the airlock to blow the dust off of the fabric, so it does not abrade the suits. In all likelihood all three strategies will be used in concert. But since the nature of the surfaces of both the dust and spacecraft surfaces are different in the lunar environment than they are in the ambient terrestrial environment, these technologies must be verified in a high fidelity lunar environment simulation chamber.

The lunar dust adhesion bell jar (LDAB) has been built at the NASA Glenn Research Center to provide a high fidelity simulation of the lunar surface environment. Although the principal mission of LDAB is to study the adhesion of lunar dust to spacecraft surfaces, it has been designed with the flexibility to study the effects of lunar dust on the functional properties of candidate materials and surfaces as well. A cut-away drawing of the LDAB is illustrated in Figure 1. A thorough discussion of the LDAB subsystems has been undertaken elsewhere (ref. 9).

The first series of experiments carried out in the LDAB were designed to determine the extent to which lunar dust will degrade the performance of thermal control surfaces. In essence, a plot must be developed with the percent dust coverage on the ordinate, and the degradation of thermal performance on the abscissa. In practice, neither of the quantities to be plotted were straightforward. It is the object of this paper to describe the difficulties in determining the percent dust coverage and the thermal degradation, and how they were overcome. It is hoped that lessons learned in this application might be fruitfully applied to others.

PERCENT DUST COVERAGE DETERMINATION

The samples tested utilized either a white thermal control paint (AZ-93) or a second surface mirror (Ag coated FEP Teflon (Dupont)) as the thermal control surface. The thermal control surface was applied either to 2.54 cm (1 in.) diameter aluminum substrates, or to identically fabricated composite samples. The composites, which were fabricated in-house, contained a surface layer of K-1100 high thermal conductivity graphite fibers and enough layers of PAN-based structural carbon fibers to give a thickness of 6.4 mm (0.25 in.) in a matrix of RS-3 isocyanate resin. This is the same composite structure used by the thermal control group for composite radiators within the ETDP's Fission Surface Power project. The laminate was laid up as a single sheet and then the round disks were machined from that sheet. The AZ-93 paint was applied by AZ Technology (Huntsville). The AgFEP samples were fabricated by Sheldahl (Northfield, MN) from 12.7 μm (5 mil) thick FEP Teflon which was coated with a few tens of nm of silver and a few tens of nm of inconel as a sealing layer to prevent oxidation. They were hand-applied to the samples using adhesive.
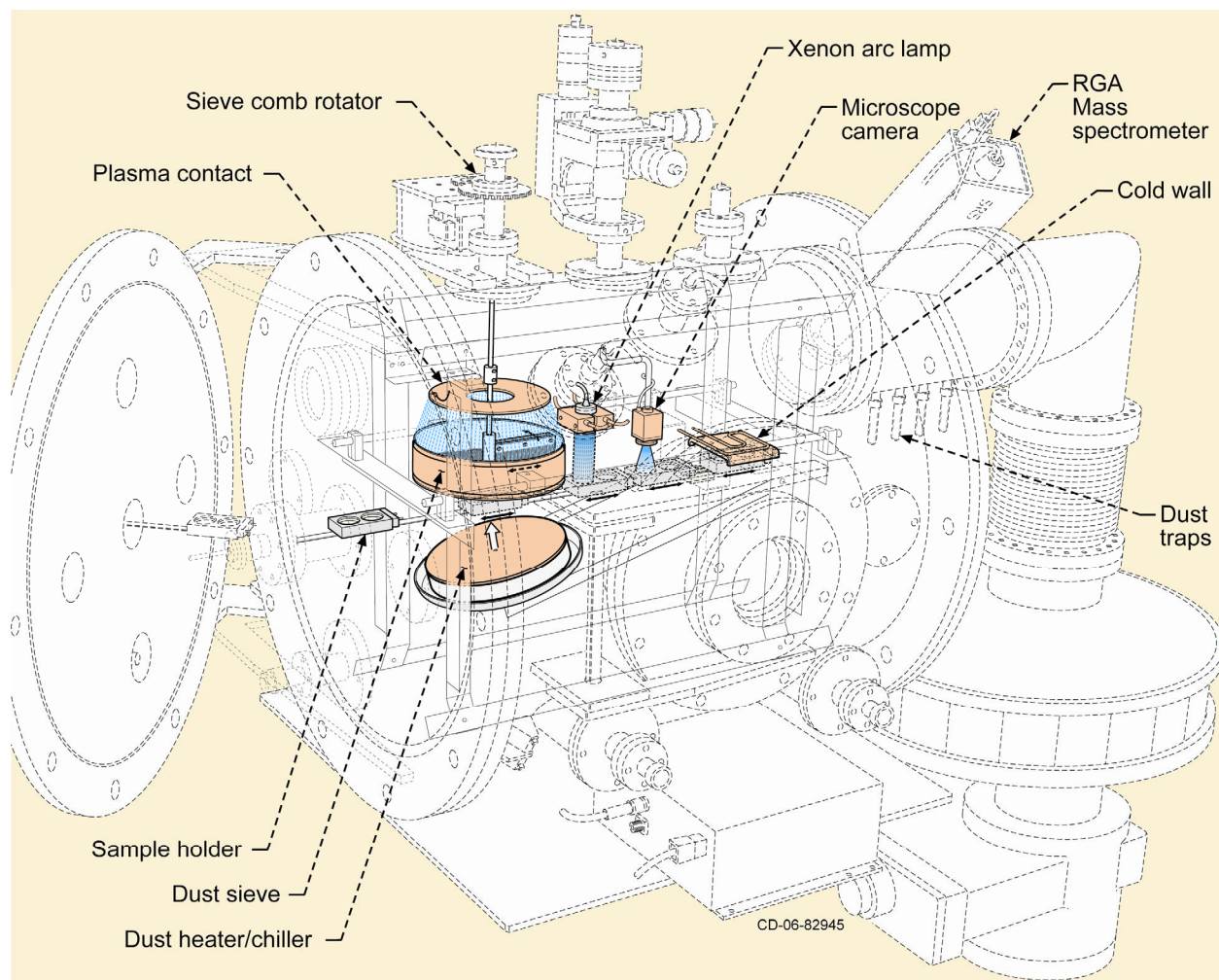
Figure 1.—Cutaway drawing of the lunar dust adhesion bell jar (LDAB) showing the location of the major subsystems.

Lunar dust proved to be much more cohesive and adhesive than similar dust on Earth. This is thought to be because the surface of lunar dust is free of water molecules, and probably chemically activated as well. Without the surface layer of water, the particles can come into closer contact which enhances cohesion and adhesion. These "clean body" effects have been well-characterized with other materials subjected to ultrahigh vacuum and indeed on returned lunar samples as well (ref. 10). The LDAB is designed to produce these same effects on lunar simulant materials for high fidelity materials testing.

Lunar simulant dust is loaded into a bowl within the LDAB where it is conditioned so that it might be more lunar like. This conditioning starts by pumping on the chamber with a mechanical roughing pump while intermittently stirring the dust until the vacuum reaches 10^{-1} Torr. At this point a radio frequency air plasma is ignited which generates oxygen ions and ultraviolet light which cleans organic contaminants off of the dust for at least 1 hr. This is followed by heating the dust to 200 °C and the chamber to 60 °C over night while pumping on the chamber with an oil diffusion pump equipped with a liquid nitrogen cold trap to remove adsorbed water. After cooling, a vacuum of 7×10^{-8} Torr is typically attained. The samples are moved into position under a well-collimated, unfiltered Xe arc lamp to mimic

solar radiation in the near ultraviolet, visible, and infrared portions of the spectrum. The lamp is located inside the chamber to avoid losses in the ultraviolet region due to absorption by window material. The temperatures of the samples were monitored using type K thermocouples mounted to their back sides and after exposure for 15 min or until the temperature reached 200 °C. The lamp is then turned off and the sample is moved into an absorbent-lined copper cold box that is maintained at about 30 K with a recirculating helium refrigerator. The temperature is monitored until the sample reaches equilibrium. The samples are then pulled out of the cold box and allowed to come to room temperature.

The pressure is increased back to 10^{-1} Torr by backfilling with a non-flammable hydrogen-helium mixture and a second plasma is ignited for 1 hr. This chemically reduces the surface of the dust and implants some hydrogen into the dust as well. After the plasma treatment, the vacuum is re-established and typically drops to about 2×10^{-7} Torr. *In situ*, the dust is dumped from the bowl into a standard 7.6 cm (3 in.) screen of 25 or 32 μm size. The samples are positioned underneath the sieve, and dust is deposited on them by mechanically shaking the sieve. This is to limit the size of the dust deposited onto the samples to the fine fraction.

If successfully treated, the cohesion and adhesion of the dust should be enhanced significantly. Unfortunately, the dust is so cohesive it does not sieve well. It proved surprisingly difficult to apply an even coating of dust on thermal control surface samples. It was thought that a simple sinusoidal motion of the sieve would deposit the dust evenly and reproducibly. This has proven not to be the case. Varieties of jarring and vibrating motions were also employed, but did not give consistently even coatings. To complicate the problem further, once the dust has been treated *in vacuo* it behaved differently than it did in the tests that were conducted in air. Schemes that would work on one run would not work on the next. Time that the dust was sifted onto the sample correlated very poorly with the amount of dust deposited. That is, more dust may be deposited in a 60 sec run than on a 600 sec run. Typical results are shown in Figure 2. It can be readily seen that the left sample has much more dust deposited on it than the right sample.

The characterization of fractional coverage by dust is complicated by the fact that all particles deposited on the samples are smaller than 32 μm, because of the sieve. Thus, although the right hand sample in Figure 2 appears to be clean, microscopic investigation reveals that about 5 percent of its surface is covered with dust, and indeed its absorptance is increased.
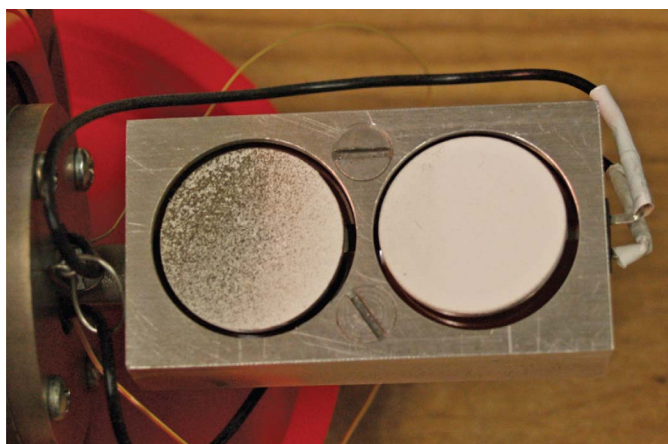

Figure 2.—Photograph of two AZ-93Al-1 samples that were dusted at the same time in the configuration shown. The left hand sample, particularly on its left half, was coated much more heavily than the right hand sample.

Determining the fractional occultation of the thermal control surface by a sub-monolayer of sub-25 μm particles is not straightforward. The sample disks have an area of 5×10^8 μm^2, and the largest particles 500 μm^2. In order to count such small particles, magnification of at least 100× is required. At 100× the area imaged by our microscope is 968×726 μm, so there are 641 non-overlapping frames that are completely filled with sample disk. Frames that were partially filled with the disk were ignored. This is permissible because the pattern of the dust distribution is larger than the sample, so we are in a sense only sampling already from a larger distribution. Rather than count the particles in all 641 frames for each of 17 samples (nearly 11,000 photos!) it was decided to analyze a statistically significant random sample of the frames.

In order to take rigorously random samples, a computer controlled x-y-θ stage was installed on the microscope. Each sample was mounted on the stage with a specific orientation (i.e., the thermocouple holes aligned in the θ = 0 direction). The random number generator in Microsoft Excel (Microsoft Corporation) was used to set the θ value for each sample in order to account for systematic angular consistencies that might be present in the dust distribution pattern. The percentage of dust coverage on each sample was estimated by superimposing a grid onto each sample dividing the sample into 641 non-overlapping frames of equal size. Frames on each sample were then randomly chosen using the random number generator and each selected field was located and digitally photographed. The dust appears dark on the AZ-93 coating, but light on the AgFEP coatings, as can be seen in Figure 3. The largest particles are < 25 μm in size. Image-Pro (company name) software was used to determine the proportion of black (128 to 256 on the grey scale) to white pixels (0 to 128 on the grey scale) in each photograph. The percentage of black pixels represents the overall dust coverage of the tested field on AZ-93, and the percentage of white pixels represents the overall dust coverage of the tested field on AgFEP.

A 95 percent confidence interval (CI) was also calculated around each mean to determine the precision of the estimated mean using equation 1:

$$CI = \bar{n} \pm z\sqrt{\frac{p(1-p)}{n}} \tag{1}$$

where z is the critical value from the normal distribution (1.96 for a 95 percent CI), p is the sample proportion (percentage of pixels occulted by dust), and n is the sample size (number of frames examined) (ref. 11). Because this formula assumes a functionally infinite population, an assumption not met when over 5% of the population is being sampled, the finite population correction was applied to adjust the confidence interval calculation:

$$CI = \bar{n} \pm z\sqrt{\frac{p(1-p)}{n-1}\left(1-\frac{n}{N}\right)} \tag{2}$$

where N is the population size (total number of frames in a sample). This provides a more accurate estimate by taking into account the high percentage (> 5 percent) of samples being measured, thereby reducing the standard error.
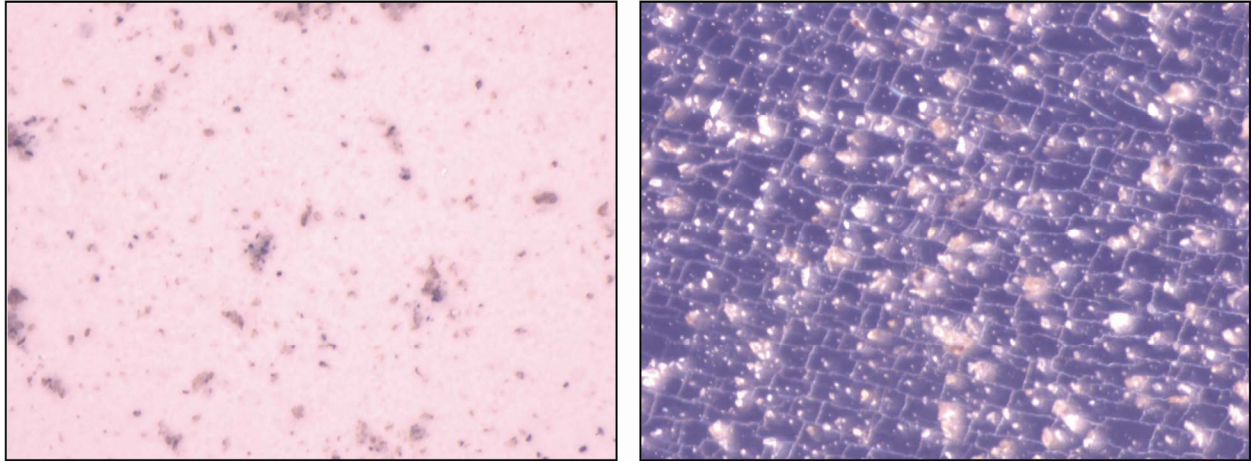
Figure 3.—Photomicrographs of the AZ-93 sample (left) and AgFEP sample (right) that were used in the analysis of fractional dust coverage. The area covers in each photomicrograph is about 1 mm^2.
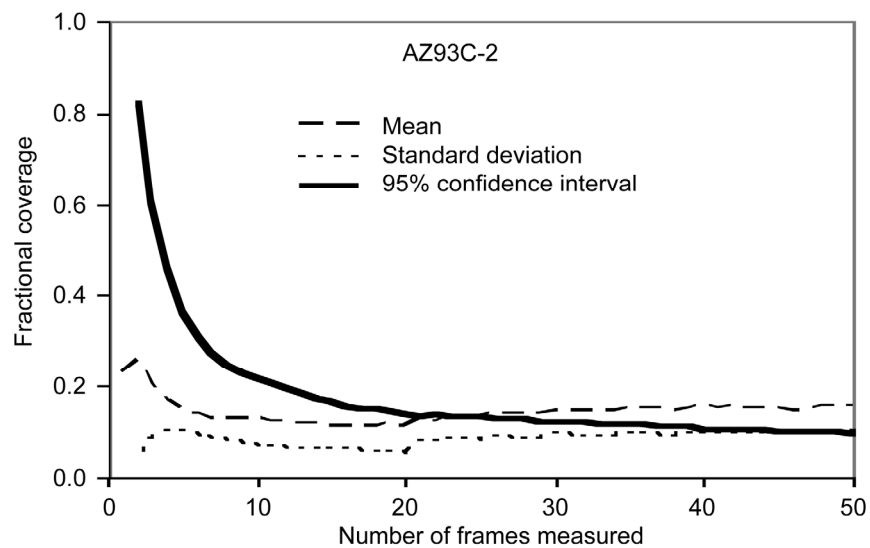
Figure 4.—Statistical parameters as a function of frames examined for dusted sample.

There is a trade-off in number of frames examined between the amount of effort and the precision which the measurement is known. The mean, standard deviation, and confidence interval as a function of frames examined for a typical sample are plotted in Figure 4. It can be seen that the 95 percent confidence interval flattens out, and measuring beyond 50 frames would have limited returns. Thus, 50 frames were measured for each sample.

Figure 5.—Plot of $\alpha/\alpha_{pristine}$ as a function of fractional dust coverage for the AZ-93Al samples. The (♦) are mean percent for each experiment and the horizontal 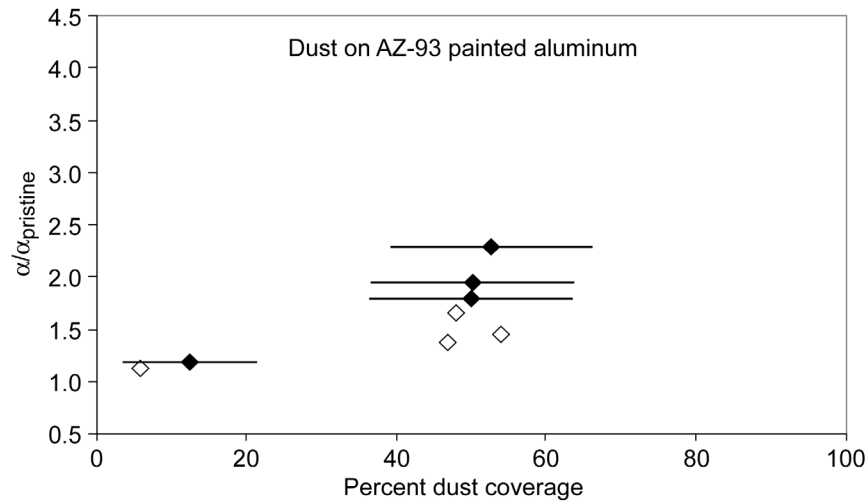lines bound the coverage at the 95 percent confidence interval. The (◇) are the dust coverage estimates from single frame measurements, combined with a simple linear model to calculate α.

The result of the calculations for dusted, AZ-93 painted aluminum is shown in Figure 5. Notice that the 95 percent confidence interval is fairly large, between 9 and 13 percent in this case, despite the fact that the mean, shown in Figure 4, seems to vary little. This was true for all four materials tested. It can be seen in equation 1 that greater numbers of measurements are required for the same confidence interval if the mean coverage is near 50 percent, than if it is near 0 or 100 percent.

THERMAL PERFORMANCE DEGRADATION DETERMINATION

The thermal modeling was done using Thermal Desktop (Cullimore & Ring Technologies), a PC based design environment for generating thermal models of electronics and vehicles. Thermal Desktop incorporates both parameter based finite difference surfaces with finite elements and CAD technology to model thermal problems. Thermal Desktop develops the capacitance and conductance network for input to SINDA/Fluint which is a comprehensive finite-difference, lumped parameter (circuit or network analogy) tool for heat transfer design analysis and fluid flow analysis in complex systems. Thermal Desktop 5.1 Patch 3 was used to generate the thermal model, which consists of 743 nodes and 1840 linear conductors. A visualization of the model and the material parameters used in it are shown in Figure 6.

Any thermal model has to be constrained. In this study, the AZ-93 coated aluminum samples were considered to be the baseline. There are many characteristics that could vary over the course of the experiment such as the intensity of the heating lamp, the translational and angular positions of the sample, and the temperature of the cold box. It was decided to hold all those variables constant, and to sweep all errors into the absorptivity (α) and the emissivity (ε) of the samples. The method for goodness of fit between the model and the data was to minimize the differences between the area under the temperature as a function of time plot, i.e., the weighted average difference. In most cases, the calculations iterated until that difference was less than 1 percent.
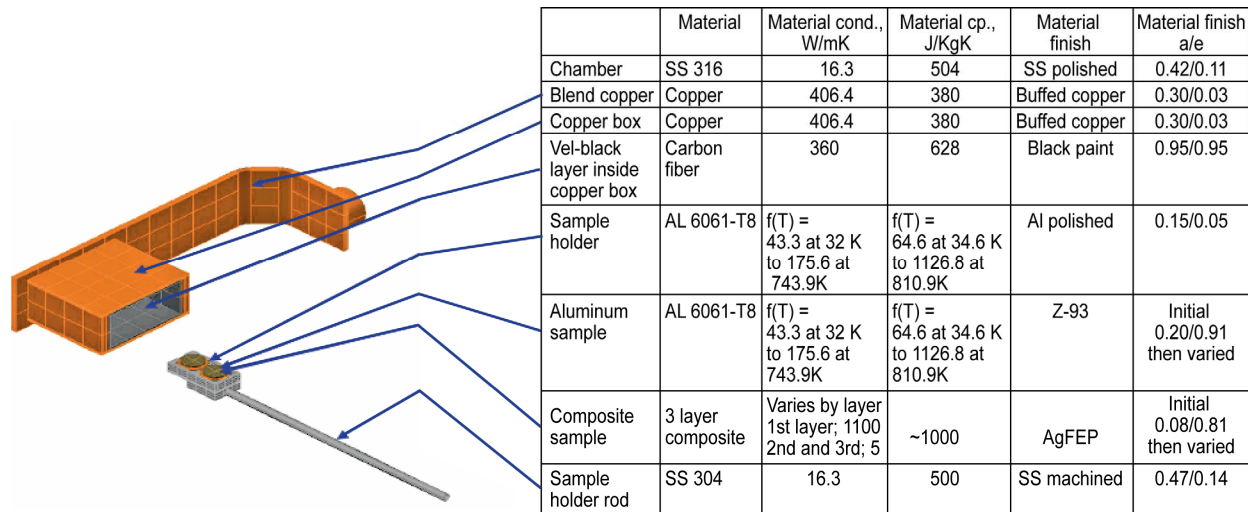
	Material	Material cond., W/mK	Material cp., J/KgK	Material finish	Material finish a/e
Chamber	SS 316	16.3	504	SS polished	0.42/0.11
Blend copper	Copper	406.4	380	Buffed copper	0.30/0.03
Copper box	Copper	406.4	380	Buffed copper	0.30/0.03
Vel-black layer inside copper box	Carbon fiber	360	628	Black paint	0.95/0.95
Sample holder	AL 6061-T8	f(T) = 43.3 at 32 K to 175.6 at 743.9K	f(T) = 64.6 at 34.6 K to 1126.8 at 810.9K	Al polished	0.15/0.05
Aluminum sample	AL 6061-T8	f(T) = 43.3 at 32 K to 175.6 at 743.9K	f(T) = 64.6 at 34.6 K to 1126.8 at 810.9K	Z-93	Initial 0.20/0.91 then varied
Composite sample	3 layer composite	Varies by layer 1st layer; 1100 2nd and 3rd; 5	~1000	AgFEP	Initial 0.08/0.81 then varied
Sample holder rod	SS 304	16.3	500	SS machined	0.47/0.14

Figure 6.—Picture of the thermal model and parameters used in its construction.

One important unknown was the radiant power of the heating lamp. An independent calibration swamped out the detector, which established that the intensity of the lamp was greater than 10 suns. The experienced technician who did the testing estimated that it might be as high as 20 suns. When it was assumed from examining the literature that the ε of the AZ-93 coated aluminum sample was 0.895, and the α was 0.172, the intensity of the lamp was found to be 29.1 kW/m^2, or about 21.5 suns. This was the value that was used for the lamp intensity for all subsequent calculations.

For the pristine samples during heating, the α and ε of the coated sample are set to their initial values. Subsequently, the α was varied for each test run until there was less than 1 percent difference in the weighted average temperatures between each test run and each analysis run. During cooling, the ε was varied for each test run until there was less that 1 percent difference in the weighted average temperatures between each test run and each analysis run.

For the dusted samples during heating, and for the same lamp power established previously, the α was varied for each test run until there was less that one percent difference in the weighted average temperatures between each test run and each analysis run. During cooling, the ε was varied for each test run until there was less that 1 percent difference in the weighted average temperatures between each test run and each analysis run.

RESULTS

A full discussion of the results is available elsewhere (ref. 12), and will only be summarized here. Table I shows the resulting values for the average of 4-7 data runs on each of the four materials tested. Note that the ε drops and the α rises when composite substrates are used, so α/ε rises as well.

By combining the statistical techniques to measure the percent dust coverage with the thermal degradation, α/ε, a plot of the thermal degradation was obtained (Figure 6). Interestingly, the degradation values seem to rise monotonically with dust coverage regardless of the thermal control coating or

substrate. A least squares line (without the outlier with a 3.68 α/ε) has an R^2 of 0.72, and extrapolates to a value of degradation of a factor 3 at full coverage by dust.

In most studies the ε of radiators has been assumed not to change in a significant way when they accumulate dust because the ε of the dust itself is so high. However, sub-monolayers of dust on AZ-93 paint lowered the ε so much that a full monolayer would have degraded the surface to 80 percent of its clean value. In contrast, sub-monolayers of dust on AgFEP surfaces raised the ε such that a full monolayer would have enhanced the ε by 20 percent. This is particularly important if the thermal control surface is in a well shaded area.

The overall degradation of the thermal control surface depends on both the α and ε. When the relative α/ε was plotted as a function of dust coverage, an interesting relationship was seen. As can be seen in Figure 2, all of the data taken together seem to rise monotonically. A least squares fit to this data has an R^2 of 0.72, and crosses the 100 percent dust coverage line at about 3. This implies that no matter which surface or substrate is used, a monolayer of dust on it will raise its α/ε by a factor of 3. Or put another way, thermal control surfaces must be made 3 times larger if they are expected to be covered with dust than if they would remain clean.

TABLE I.—OPTICAL PROPERTIES OF MATERIALS USED IN THIS STUDY

Pristine Material	Emissivity (ε)	Absorptivity (α)	α/ε
AZ-93 on Al	0.886 ± 0.024	0.173 ± 0.029	0.195
AZ-93 on composite	0.833 ± 0.027	0.196 ± 0.006	0.235
AgFEP on Al	0.719 ± 0.041	0.073 ± 0.006	0.102
AgFEP on composite	0.648 ± 0.038	0.101 ± 0.025	0.156

Figure 7.—The total change in α/ε as a function of dust coverage.
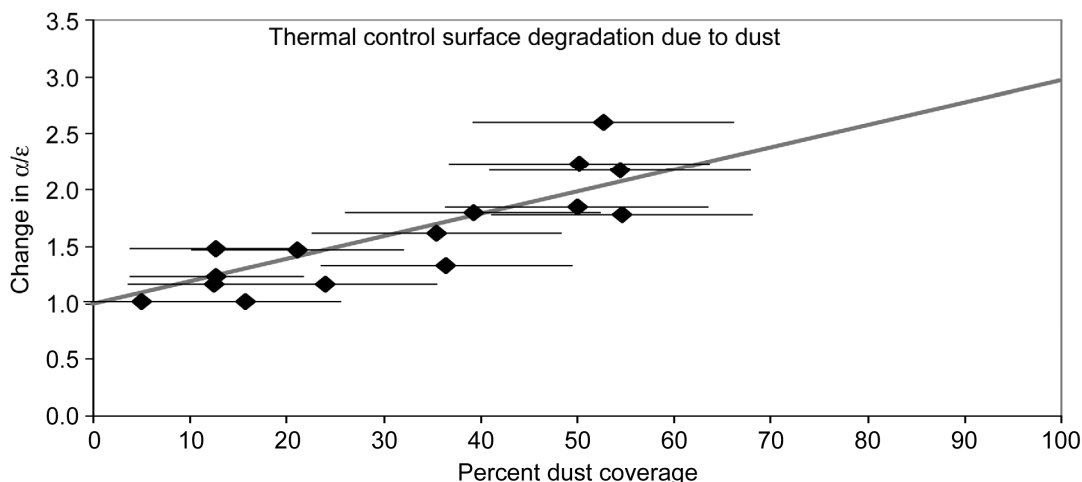
CONCLUSIONS

Challenges associated with determining the percent coverage of dust applied to samples in the LDAB have been described and a statistical method to overcome them proposed. A thermal model is described that is capable of reproducing the experimental data within 1 percent. Even though it is difficult to narrow the range of the confidence interval without taking an extraordinary number of measurements, and the α/ε values contain all other sources of error in the time temperature plots, the trends are clear nonetheless. Even sub-monolayers of lunar dust will have a significant impact on the performance of thermal control surfaces. This study suggests that full monolayer coverage will raise the α/ε values by a factor of 3 over a clean thermal control surface. Clearly, dust mitigation techniques must be developed to protect these surfaces during lunar exploration.

REFERENCES

1. G.W. Bush, "A Renewed Spirit of Discovery: The President's Vision for U.S. Space Exploration," (2004).

2. "NASA's Exploration Systems Architecture Study," NASA/TM—2005-214062.

3. J.R. Gaier, "The Effects of Lunar Dust on EVA Systems During the Apollo Missions," NASA/TM—2005-213610.

4. H. Schmitt, "The Apollo Experience/Problems Encountered with Lunar Dust," Biological Effects of Lunar Dust Workshop, Sunnyvale, CA (2005).

5. Jacobs, S., Durkee, R.E., and Harris, R.S., "Lunar Dust Deposition Effects on the Solar Absorptance of Thermal Control Materials," AIAA Paper 71–479 presented at the AIAA 6th Thermophysics Conference, Tullahoma, TN, April 1971.

6. McKay, G.H., Chairman, "Saturn V Launch Vehicle Flight Evaluation Report-AS-510, Apollo 15 Mission," Saturn V Flight Evaluation Working Group, 1971.

7. McKay, G.H., Chairman, "Saturn V Launch Vehicle Flight Evaluation Report-AS-511, Apollo 16 Mission," Saturn V Flight Evaluation Working Group, 1972.

8. McKay, G.H., Chairman, "Saturn V Launch Vehicle Flight Evaluation Report-AS-512, Apollo 17 Mission," Saturn V Flight Evaluation Working Group, 1973.

9. James R. Gaier and Edward A. Sechkar, "Lunar Simulation in the Lunar Dust Adhesion Bell Jar," Proceedings of the 45th AIAA Aerospace Sciences Meeting (2007). Also, NASA/TM—2007-214704 (2007).

10. Grossman, J.J., et al., *Microchemical, Microphysical, and Adhesive Properties of Lunar Material*, Proceedings of the Apollo 11 Lunar Science Conference, Vol. 3 (1970) pp. 2171–2181.

11. Moore, David S. and McCabe, George P., *Introduction to the Practice of Statistics*, 2nd ed ., W.H. Freeman and Company, New York, 1993, pp. 576–577.

12. Gaier, J.R., et al., *The Effect of Simulated Lunar Dust on the Absorptance, Emittance, and Operating Temperature on AZ-93 and Ag/FEP Thermal Control Surfaces*, manuscript in review (2008).